ACS Photonics

Article

Cite This: ACS Photonics 2019, 6, 1990−1995

pubs.acs.org/journal/apchd5

Quantum Confined Indium-Rich Cluster Lasers with Polarized Dual-Wavelength Output

Qingnan Yu,[†] Ming Zheng,[†] Hanxu Tai,[†] Wei Lu,[†] Yue Shi,[†] Jinghua Yue,[†] Xing Zhang,[‡] Yongqiang Ning,[‡] and Jian Wu*[,†]

[†]Department of Applied Physics, Beihang University, Beijing, 100191, China

[‡]State Key Laboratory of Luminescence and Application, Changchun Institute of Optics, Fine Mechanics and Physics, Chinese Academy of Sciences, 130033, Changchun, China

ABSTRACT: A kind of new quantum confined indium (In)-rich cluster (IRC) laser with polarized dual-wavelength output is first proposed and realized. Unlike conventional quantum well/dot lasers, its optical characteristics depend on the special IRC effect-formed quantum confined structure, in which the asymmetric distribution and various sizes of IRCs are generated due to high strains in the indium-based material system. It may lead to a special band structure suitable for synchronous dual-wavelength lasing generation. The mechanism of the laser operation is associated with independent carrier transitions and stimulated emissions from multiple local indium-based active regions, which have various areas and different indium contents due to the IRC effect. The sample uses InGaAs/GaAs/GaAsP as the kernel of lasing medium with the edge-emitting configuration, both facets of which are used as cavity mirrors. The experiment exhibits synchronous dual wavelengths of lasing at 970 and 980 nm in transverse electric (TE) polarization, with a total slope efficiency of 34.6% at a room temperature of 300 K. The result is of great significance in the development of new types of monolithic quantum confined lasers with dual-wavelength and polarization output.

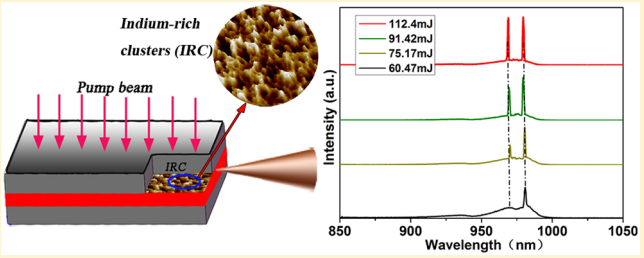

KEYWORDS: *InGaAs/GaAs, strains, quantum confined lasers, indium-rich clusters, dual wavelengths, polarization*

It is well-known that the synchronous dual-wavelength operation of semiconductor lasers has been a hot research topic in the world due to some special applications of this type of laser, for example, two-wavelength interferometry, laser medicine, difference-frequency generation of terahertz radiation, difference-frequency laser radars, and so on.[1−4] For this reason, different material systems and laser structures have been developed to achieve this goal, for example, the combination of two physically separated chips, which have different band gaps,[5] the use of double distributed Bragg reflectors (DBR),[6] the designs of a complicated external cavity with gratings or a subwavelength-thick metallic mask deposited on the top surface of the medium, which is corresponding to the antinode position of the longitudinal intracavity E-field, as a spatially distributed absorbing filter to obtain dual-wavelength lasing,[7] or the uses of an intracavity Fabry−Perot etalon, as well as coupled cavities.[8−11] These previous structures and approaches result in relatively complicated and expensive integrations. Theoretically, the design of multiple strained quantum wells may also achieve polarized dual-wavelength lasing in a single structure.[12] However, it is actually difficult to ensure the stability of synchronous dual-wavelength lasing operation with multiple strained wells due to carrier recombination competition in sub-bands. Thus, it is much desired to achieve the stable dual-wavelength lasing in a simpler monolithic structure. Unfortunately, there has not been a remarkable advance in this area to date, as the current semiconductor lasers are still designed with conventional quantum confined structures.

On the other hand, the cluster lasers running with polarization and dual wavelengths in the waveband of 900−1000 nm have never been reported yet, so far. The current cluster lasers only operate at a single wavelength in the terahertz waveband, based on laser-induced clusters,[13] or operate at a single wavelength of 1.5 μm by the saturated absorption effect from the ion-implantation-induced nanostructure clusters,[14] as well as operate at a single wavelength in the X-ray waveband by laser-cluster interaction, etc.[15]

In this paper, we are reporting a special and very interesting quantum confined In-rich cluster (IRC) lasers, with which stable dual-wavelength and polarized lasing in the waveband of 900−1000 nm is obtained. The laser is innovatively designed by utilizing the InGaAs/GaAs-generated IRC effect. Since a high strain generated from a large lattice mismatch between InGaAs and GaAs materials can cause indium atoms to migrate along the growth direction in the InGaAs/GaAs material system, a large number of clusters may be formed on the surface of InGaAs layer to relax the high strain in the system when InGaAs is grown over a few monolayers in thickness on

Received: March 15, 2019
Published: July 1, 2019

DOI: 10.1021/acsphotonics.9b00406
ACS Photonics 2019, 6, 1990−1995

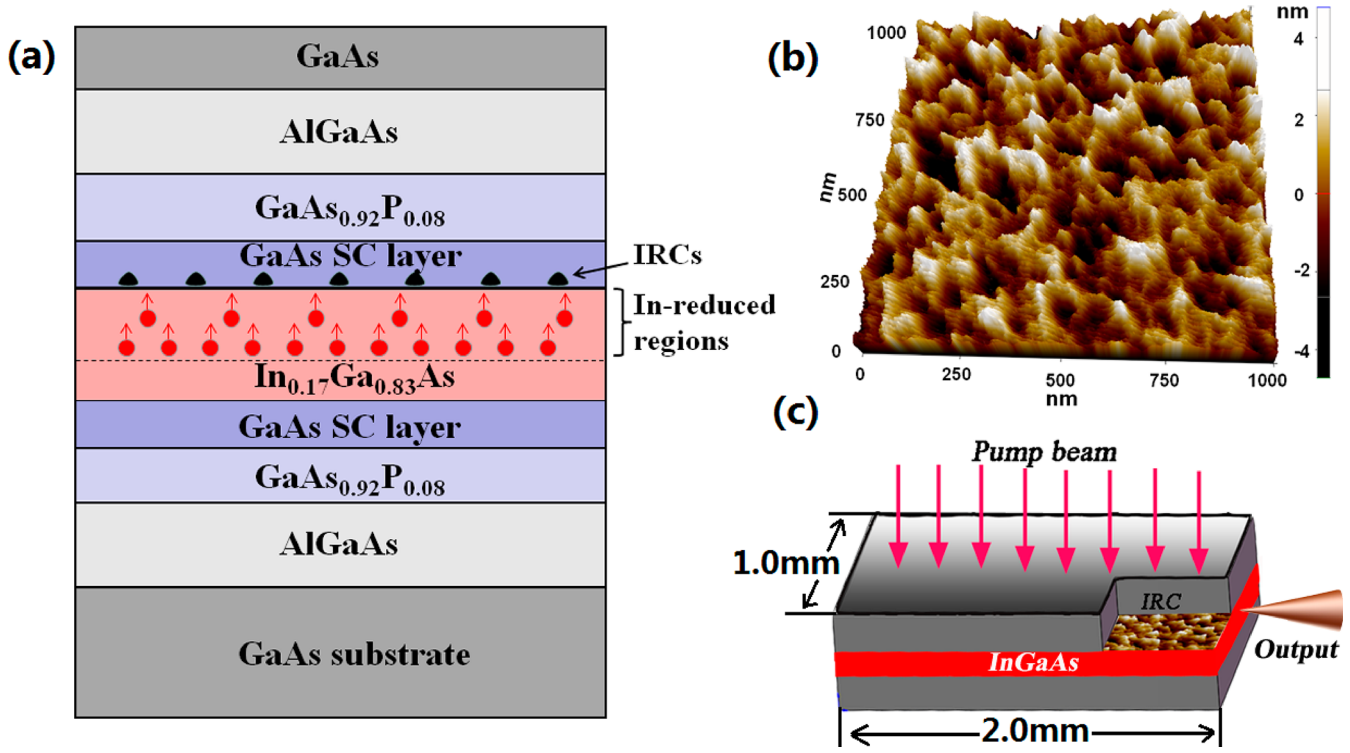

Figure 1. (a) Laser structure and fundamental principle of the IRC formation, in which AlGaAs is the waveguide layer. (b) IRC structure photograph from an AFM. (c) Edge-emitting IRC laser configuration, where the red part is the InGaAs active layer and the gray parts are all the layers exclusive of the InGaAs active layer, as shown in (a).

the GaAs layer.[16−18] As a result, the migration of the indium atoms (the formation of IRCs) leads to loss of the indium contents from the corresponding InGaAs regions. So multiple discrete InGaAs active regions with different areas and indium contents are formed. This results in an unusual stimulated emission mechanism for the polarized dual-wavelength lasing generation.

IRC LASER STRUCTURE

The epitaxial structure of the indium-based IRC laser sample is grown on the GaAs (001) substrate using metal organic chemical vapor deposition (MOCVD) technique, as shown in Figure 1a. The basic active layer material is $In_{0.17}Ga_{0.83}As$, with a thickness of 10 nm, where the 10 nm thick $In_{0.17}Ga_{0.83}As$ layer is designed here to generate necessary strain accumulation for the IRC's formation. This is because the thickness and indium content of the $In_xGa_{1-x}As$ layer are two key factors of the IRC formation.[16] An additional 2 nm thick GaAs strain-compensating (SC) layer is embedded next to the $In_{0.17}Ga_{0.83}As$ active layer to assist the IRC's formation and control the strain between InGaAs and barrier layers. Both of them are sandwiched by 8 nm thick $GaAs_{0.92}P_{0.08}$ barriers. Beyond the InGaAs/GaAs/GaAsP kernel are the AlGaAs waveguide layers, the GaAs top cap, and the GaAs (001) substrate. The sample is deposited at a rate of 0.75 $\mu m \cdot h^{-1}$ and 100 mbar in pressure. A high temperature of 660 °C is applied to increase the migration length of the indium atoms, which will be helpful to the IRC's formation in the material growth.[19] The V/III ratio of the materials is 40 for the structure growth.

The IRCs formed on the InGaAs surface are observed and measured using an atomic force microscope (AFM; Park Systems Instrument Co., Ltd., Model XE100). The result is shown in Figure 1b, in which the clusters can roughly be divided into two scales of 150 and 50 nm. Thus, the indium contents of the local $In_xGa_{1-x}As$ regions corresponding to the cluster locations are reduced from $x = 0.17$ down to two different levels accordingly.

The IRC samples are fabricated in an edge-emitting configuration with 1.0 mm × 2.0 mm in area here, both facets of which are used as F−P cavity mirrors without coating for lasing generation. The reflectivity of the facets are $R = 30\%$. It is determined by the InGaAs index, as shown in Figure 1c, where red and gray parts denote the InGaAs active layer and the layers exclusive of the InGaAs layer, respectively. The sample is vertically pumped using 808 nm pulsed laser (a product of Beijing Laserwave Optoelectronics Technology Co. Ltd., Model LWIRL808-40W-F) with a pulse width of 20 ms under the room temperature of 300 K. The use of pulsed laser is to avoid the thermal effect. The experimental setup for the measurement of photoluminescence (PL) and dual-wavelength lasing is described in Figure 2, in which a linear polarizer P and

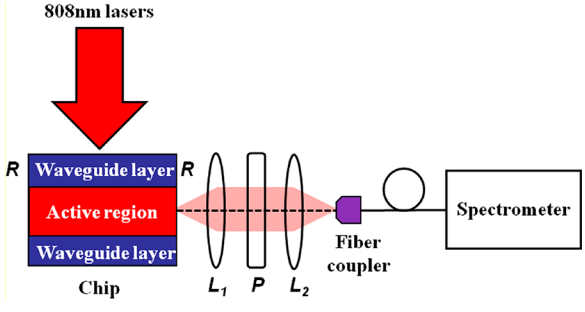

Figure 2. Experimental setup for PL and dual-wavelength lasing measurement from the facets of the sample.

DOI: 10.1021/acsphotonics.9b00406
ACS Photonics 2019, 6, 1990−1995

two lenses of L_1 and L_2 are used for collection of the emissions in different polarization modes from the facets of the sample. The signals are detected using a spectrometer (Ocean Optical Co. Inc., HR4000CG-UV-NIR) coupled with a fiber. In order to measure PL spectra of the IRC laser structure, the sample is coated with a transmittance of 99.99% at one end and uncoated at the other end in experiment.

The theoretical analysis points out that the lasing mechanism of the IRC laser structure is quite different from that of the conventional quantum well/dot lasers and the previous cluster lasers. First, the stimulated emission does not come from the IRCs. Instead, it comes from all the InGaAs regions, which have various sizes and indium contents due to the IRC effect. Since the IRCs consist of indium atoms or InAs rather than InGaAs compounds, these IRCs do not contribute to the emissions ranging in 850−1050 nm. This is because the unstrained InAs compound has the band gap of 0.35 eV, which is corresponding to the emission wavelength of 3.5 μm. Also, the compressively strained InAs/GaAs quantum dots produce the emission at the peak wavelength of 1.3 μm due to a large lattice mismatch.[20,21] The clusters' role in the IRC laser structure is the nonuniform reduction of Indium content of the $In_xGa_{1-x}As$ compound to form many discrete and indium-reduced InGaAs regions. These regions, together with the unaffected InGaAs part, constitute the whole active layer.

RESULTS AND ANALYSIS

Figure 3 analyzes the measured PL spectrum from the IRC sample. The injection energy is 112.4 mJ. Three peaks are

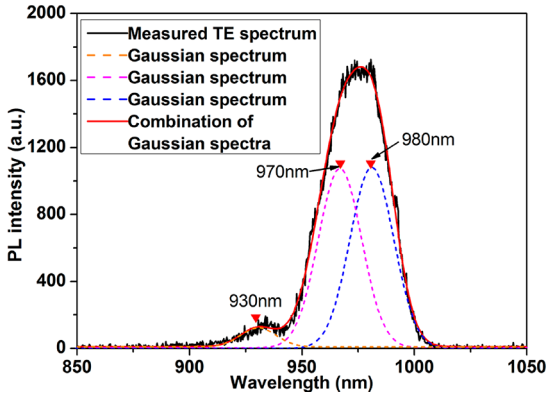

Figure 3. PL spectrum analysis with the experimental data and Gaussian simulations for the $In_{0.17}Ga_{0.83}As$, $In_{0.15}Ga_{0.85}As$, and $In_{0.12}Ga_{0.88}As$ materials under a pulsed optical injection of 112.4 mJ.

observed in the measured PL spectrum, in which two extra peaks appear due to the emissions from the $In_{0.15}Ga_{0.85}As$ and $In_{0.12}Ga_{0.88}As$ regions.[22] With the Gaussian simulation, it is found that the combination of three Gaussian spectra with peaks at 980, 970, and 930 nm is exactly identical to the experimental PL spectrum. It indicates that these three Gaussian spectra describe the PL emissions from the $In_{0.17}Ga_{0.83}As$, $In_{0.15}Ga_{0.85}As$ and $In_{0.12}Ga_{0.88}As$ materials, respectively, where the PL intensities at 980 and 970 nm are nearly equal to each other. This unusual result offers a chance on achieving synchronous dual-wavelength lasing with a simple F−P cavity. This is further verified by subsequent measurement and analysis of the gain and lasing spectra of the sample. The PL spectra in different polarization modes and dual-wavelength lasing intensities at 970 and 980 nm with various injection levels are measured at a room temperature of 300 K. The results are shown in Figure 4.

Figure 4a shows that the PL intensity is increased more rapidly at 970 nm than at 980 nm for the TE polarization. This is because the 970 nm emission is generated due to the carrier recombination from the higher energy levels in the two sub-bands formed in $In_{0.17}Ga_{0.83}As$ and $In_{0.15}Ga_{0.85}As$ materials, respectively, while the 980 nm emission comes from the carrier recombination at lower energy levels only in the sub-band of the $In_{0.17}Ga_{0.83}As$ material. Thus, more carriers are contributed to the 970 nm emission, as the injection is increased. Eventually, both of the emissions will be saturated when the sub-bands are fully occupied by carriers. In addition, the 970 and 980 nm emissions come from the carrier recombination between the first conduction sub-band, C_1, and the first valence sub-band of heavy holes, HH_1, in the $In_{0.17}Ga_{0.83}As$ and $In_{0.15}Ga_{0.85}As$ materials, respectively. Thus, both of the emissions are in the TE polarization mode. These can be understood by Figure 5b and are verified by the experimental results in Figure 4b. In order to understand the mechanism of the dual-wavelength lasing generated in the IRC laser structure, the modal gain is measured and analyzed in Figure 5a as well. The details of the gain measurement approach refer to the articles.[22,23] Also, the special band structure in the IRC laser is analyzed in Figure 5b.

A special band structure with two different band gaps and Fermi distributions of the carriers is formed due to the IRC effect, in which alternate compressive and tensile strains exist, as shown in Figure 5b. The $In_xGa_{1-x}As$ regions with different indium contents of x = 0.17, 0.15, and 0.12 result in the step-like sub-bands or barriers. It looks like a model consisting of two compressively strained wells, in which inside barriers show much lower heights than outside barriers for both of the wells. Thus, both of the wells can obtain the carriers for recombination when the injection energy is higher than the inside barrier height. This is the key point to obtain stable dual-wavelength lasing and different from the classic multiple well structure, in which all wells have the same barrier heights so that it is difficult to obtain a stable dual-wavelength lasing due to the carrier recombination competition. The details of the dual-wavelength lasing process are described as follows. The $In_{0.17}Ga_{0.83}As$ sub-band is first filled by carriers, when the optical injection is at a lower level, because it has the lowest potential energy or the smallest band gap. Thus, lasing occurs at 980 nm at first. With the increase of injection, the $In_{0.15}Ga_{0.85}As$ sub-band and the higher energy levels in the $In_{0.17}Ga_{0.83}As$ sub-band are filled by carriers, and lasing at 970 nm occurs as well. Since the stimulated emission at 970 nm comes from the carrier recombination in both $In_{0.17}Ga_{0.83}As$ and $In_{0.15}Ga_{0.85}As$ sub-bands, but the stimulated emission at 980 nm happens only relating to the $In_{0.17}Ga_{0.83}As$ sub-band, the lasing intensity is increased more rapidly at 970 nm than at 980 nm with increasing the optical injection. This is verified by the experimental result in Figure 4b.

In addition, both of the stimulated emissions at 970 and 980 nm come from the compressively strained regions of the $In_{0.17}Ga_{0.83}As$ and $In_{0.15}Ga_{0.85}As$ materials. Hence, the dual-wavelength stimulated emissions are in TE polarization mode. This can be further illustrated with the modal gain, which is experimentally obtained in Figure 5a, where the threshold gain of G_{th} is given by 15.04 cm^{-1} here. It is distinctly shown that the effective gain spectrum is the combination of all gains from different $In_{0.17}Ga_{0.83}As$, $In_{0.15}Ga_{0.85}As$, and $In_{0.12}Ga_{0.88}As$

DOI: 10.1021/acsphotonics.9b00406
ACS Photonics 2019, 6, 1990−1995

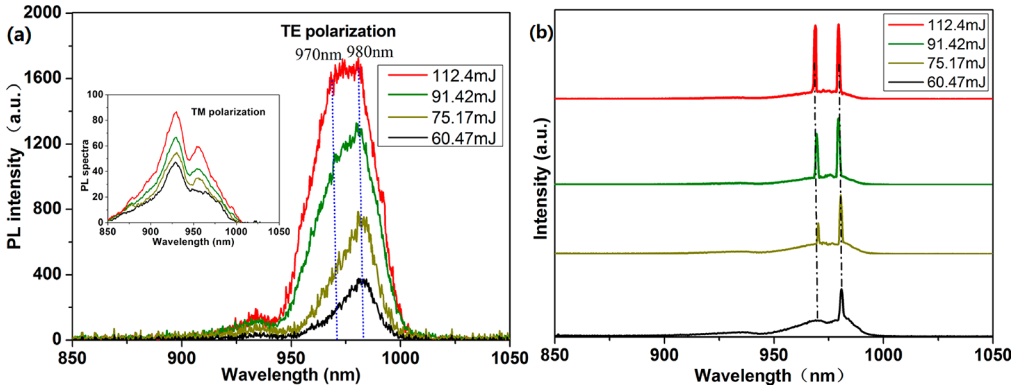

Figure 4. (a) Measured PL spectra in TE and transverse magnetic (TM) polarizations with various optical injections. (b) TE-polarized lasing intensities at 970 and 980 nm with various optical injections.

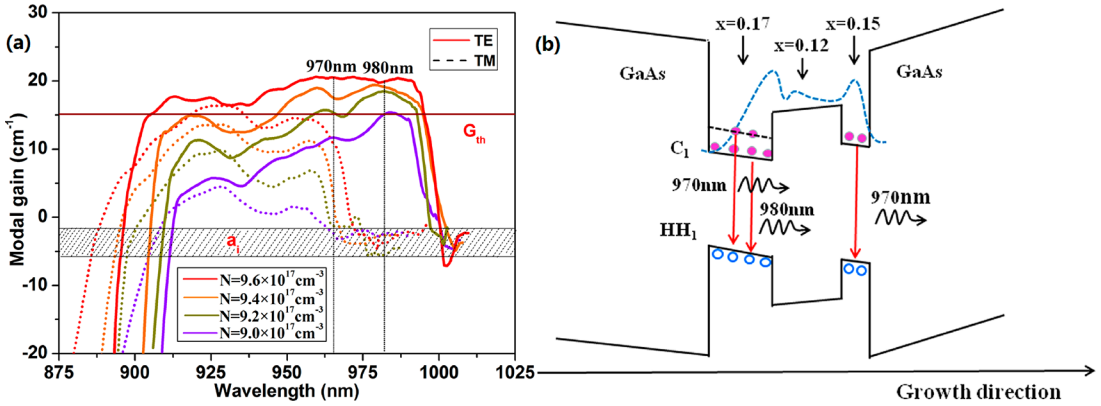

Figure 5. (a) TE and TM modal gains from various optical injections. (b) Special band structure with different sub-bands and band gaps due to compressive and tensile strains in the IRC laser.

regions. Since the maximum peak appears at 980 nm in the TE gains, lasing occurs at 980 nm with TE mode at first. As the injection is increased, the gain peak at 970 nm subsequently appears above the threshold, and lasing at 970 nm with TE mode is obtained as well. Both of the stimulated emissions are just corresponding to the two separated compressively strained sub-bands, as shown in Figure 5b. Thus, lasing with the dual wavelengths of 970 and 980 nm and TE polarization is obtained. The other modes, including the TM polarization, fail to obtain the effective gain due to the mode competition effect.

The input−output characteristics of the dual-wavelength IRC laser are measured and shown in Figure 6, in which the total slope efficiency reaches 34.6% and lasing at 980 nm reaches roll-over at first with a pulse width of 20 ms.

At last, the thermal characteristics of the TE-polarized dual-wavelength IRC laser are experimentally observed. The result is shown in Figure 7a. It shows that lasing is more sensitive to the temperature at 970 nm than at 980 nm, as a faster thermal attenuation happens at 970 nm. This is because the emission at 970 nm is corresponding to the larger band gap in the $In_{0.15}Ga_{0.85}As$ material, which will lead to more carriers to escape from the quantum confined structure. Meanwhile, the thermal effect also causes lasing wavelengths to move to the long wavelength direction, as shown in Figure 7. This is because heating makes the band gap of the material to become smaller.[24,25] Figure 7b shows that the 980 and 970 nm emissions have slightly different thermal-shifting rates of 0.32 and 0.275 nm·K^{-1}, because heating-induced band gap variation

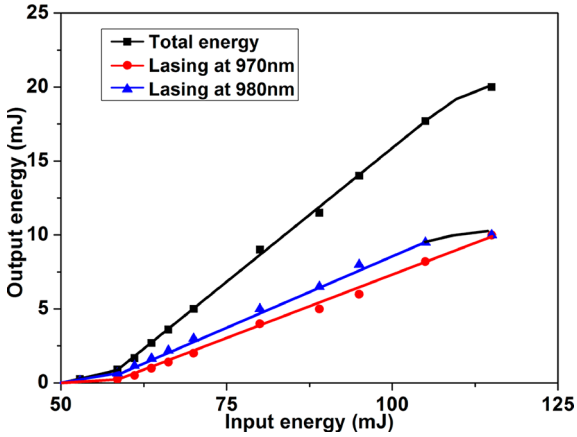

Figure 6. Input−output characteristics of the polarized dual-wavelength InGaAs/GaAs IRC laser.

is associated with the indium content in the $In_xGa_{1-x}As$ material.[26]

CONCLUSIONS

In summary, a novel InGaAs-based quantum confined IRC laser with TE-polarized dual-wavelength output is first proposed and realized. The monolithic laser structure is constructed based on the IRC effect, which can generate the asymmetric distribution and various sizes of IRCs due to the high strain formed within the InGaAs/GaAs material system. These irregular IRCs lead to multiple discrete InGaAs active

DOI: 10.1021/acsphotonics.9b00406
ACS Photonics 2019, 6, 1990−1995

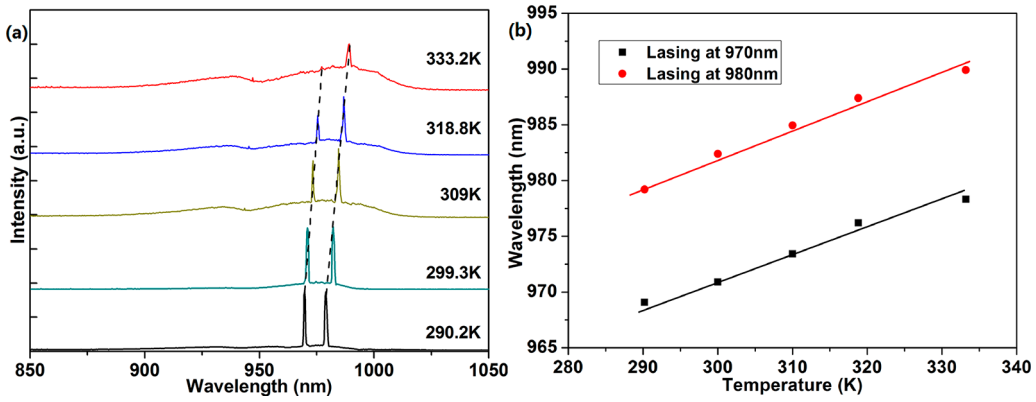

Figure 7. (a) Thermal performance of the TE-polarized dual-wavelength IRC laser structure with different temperatures. (b) Red-shift of the lasing wavelengths.

regions, which have different Indium contents reduced and strains. Unlike the conventional quantum well/dot lasers, this special IRC structure leads to a complex band structure suitable for the TE-polarized dual-wavelength lasing generation. This is associated with independent carrier transitions and stimulated emissions from multiple InGaAs active regions with different Indium contents. The sample uses InGaAs/GaAs/GaAsP as the kernel of the laser medium with an edge-emitting configuration, both facets of which are used as F−P cavity mirrors. The experiment shows that the dual wavelengths of 970 and 980 nm of lasing are observed with the total energy of 20 mJ in TE polarization mode from the optical injection of 118 mJ at room temperature. The result is of great significance in the development of new types of monolithic and polarized dual-wavelength lasers.

AUTHOR INFORMATION

Corresponding Author

*E-mail: jwu2@buaa.edu.cn.

ORCID

Jian Wu: 0000-0002-0635-3857

Notes

The authors declare no competing financial interest.

ACKNOWLEDGMENTS

The authors gratefully acknowledge the financial support of the National Natural Science Foundation of China (Grant Nos. 61376067 and 61474118) for this work.

REFERENCES

(1) Siebert, K. J.; Quast, H.; Leonhardt, R.; Löffler, T.; Thomson, M.; Bauer, T.; Roskos, H. G.; Czasch, S. Continuous-wave all-optoelectronic terahertz imaging. *Appl. Phys. Lett.* **2002**, *80*, 3003−3005.

(2) Jágerská, J.; Jouy, P.; Hugi, A.; Tuzson, B.; Looser, H.; Mangold, M.; Beck, M.; Emmenegger, L.; Faist, J. Dual-wavelength quantum cascade laser for trace gas spectroscopy. *Appl. Phys. Lett.* **2014**, *105*, 161109.

(3) Shang, Y.; Ye, X.; Cao, L.; Song, P.; Feng, J. Coaxial Dual-wavelength Interferometric Method for a Thermal Infrared Focal-plane-array with Integrated Gratings. *Sci. Rep.* **2016**, *6*, 25993.

(4) Mei, J.; Zhong, K.; Wang, M.; Liu, Y.; Xu, D.; Shi, W.; Wang, Y.; Yao, J.; Norwood, R. A.; Peyghambarian, N. Widely-tunable high-repetition-rate terahertz generation in GaSe with a compact dual-wavelength KTP OPOaround 2 μm. *Opt. Express* **2016**, *24*, 23368−23375.

(5) Zhu, R.; Wang, S. S.; Qiu, X. L.; Chen, X. H.; Jiang, M. H.; Guo-Yu, H. Y.; Zhang, P.; Song, Y. R. InGaAs quantum well based dual-wavelength external cavity surface emitting laser for wideband tunable mid-infrared difference frequency generation. *J. Lumin.* **2018**, *204*, 663−667.

(6) Shutts, S.; Smowton, P. M.; Krysa, A. B. Dual-wavelength InP quantum dot lasers. *Appl. Phys. Lett.* **2014**, *104*, 241106.

(7) Paquet, R.; Blin, S.; Myara, M.; Gratiet, L. L.; Sellahi, M.; Chomet, B.; Beaudoin, G.; Sagnes, I.; Garnache, A. Coherent continuous-wave dual-frequency high-Q external-cavity semiconductor laser for GHz-THzapplications. *Opt. Lett.* **2016**, *41*, 3751−3754.

(8) Lin, C. F.; Chen, M. J.; Lee, B. L. Wide-range tunable dual-wavelength semiconductor laser using asymmetric dual quantum wells. *IEEE Photonics Technol. Lett.* **1998**, *10*, 1208−1210.

(9) Fan, L.; Fallahi, M.; Hader, J.; Zakharian, A. R.; Moloney, J. V.; Stolz, W.; Koch, S. W.; Bedford, R.; Murray, J. T. Linearly polarized dual-wavelength vertical-external-cavity surface-emitting laser. *Appl. Phys. Lett.* **2007**, *90*, 181124.

(10) Pellandini, P.; Stanley, R. P.; Houdre, R.; Oesterle, U.; Ilegems, M.; Weisbuch, C. Dual-wavelength laser emission from a coupled semiconductor microcavity. *Appl. Phys. Lett.* **1997**, *71*, 864−866.

(11) Carlin, J. F.; Stanley, R. P.; Pellandini, P.; Oesterle, U.; Ilegems, M. The dual wavelength bi-vertical cavity surface emitting laser. *Appl. Phys. Lett.* **1999**, *75*, 908−910.

(12) Leinonen, T.; Morozov, Y. A.; Härkönen, A.; Pessa, M. Vertical external-cavity surface-emitting laser for dual-wavelength generation. *IEEE Photonics Technol. Lett.* **2005**, *17*, 2508−2510.

(13) Singh, R. K.; Singh, M.; Rajouria, S. K. High-power terahertz radiation generation by beating of two co-propagating super-Gaussian laser beams in cluster plasma. *Laser Phys.* **2018**, *28*, 1−7.

(14) Venus, G. B.; Gubenko, A.; Portnoi, E. L.; Avrutin, E. A.; Frahm, J.; Kubler, J.; Schelhase, S. The use of nanostructure-cluster-based ion-implantation-induced saturable absorbers in multisect ion high-power 1.5-μm picosecond laser diodes. *Proc. SPIE* **2012**, *5023*, 383−386.

(15) Petrov, G. M.; Davis, J.; Velikovich, A. L. Tunable synchrotron radiation from high intensity laser-cluster interaction. *J. Phys. B: At., Mol. Opt. Phys.* **2006**, *39*, 4617−4625.

(16) Jasik, A.; Wnuk, A.; Wojcik-Jedlinska, A.; Jakiela, R.; Muszalski, J.; Strupinski, W.; Bugajski, M. The influence of the growth temperature and interruption time on the crystal quality of InGaAs/GaAs QW structures grown by MBE and MOCVD methods. *J. Cryst. Growth* **2008**, *310*, 2785−2792.

(17) Schlenker, D.; Miyamoto, T.; Chen, Z.; Koyama, F.; Iga, K. Growth of highly strained GaInAs/GaAs quantum wells for 1.2 μm wavelength lasers. *J. Cryst. Growth* **2000**, *209*, 27−36.

(18) Yu, H. P.; Roberts, C.; Murray, R. Influence of indium segregation on the emission from InGaAs/GaAs quantum wells. *Appl. Phys. Lett.* **1995**, *66*, 2253−2255.

DOI: 10.1021/acsphotonics.9b00406
ACS Photonics 2019, 6, 1990−1995

(19) Muraki, K.; Fukatsu, S.; Shiraki, Y.; Ito, R. Surface segregation of In atoms during molecular beam epitaxy and its influence on the energy levels in InGaAs/GaAs quantum wells. *Appl. Phys. Lett.* **1992**, *61*, 557−559.
(20) Chen, S. M.; Tang, M. C.; Jiang, Q.; Wu, J.; Dorogan, V. G.; Benamara, M.; Mazur, Y. I.; Salamo, G. J.; Smowton, P.; Seeds, A.; Liu, H. Y. InAs/GaAs Quantum-Dot Superluminescent Light-Emitting Diode Monolithically Grown on a Si Substrate. *ACS Photonics* **2014**, *1*, 638−642.
(21) Jung, D.; Zhang, Z. Y.; Norman, J.; Herrick, R.; Kennedy, M. J.; Patel, P.; Turnlund, K.; Jan, C.; Wan, Y. T.; Gossard, A. C.; Bowers, J. E. Highly Reliable Low-Threshold InAs Quantum Dot Lasers on On-Axis (001) Si with 87% Injection Efficiency. *ACS Photonics* **2018**, *5*, 1094−1100.
(22) Yu, Q. N.; Li, X.; Jia, Y.; Lu, W.; Zheng, M.; Zhang, X.; Ning, Y. Q.; Wu, J. InGaAs-based well-island composite quantum-confined structure with superwide and uniform gain distribution for great enhancement of semiconductor laser performance. *ACS Photonics* **2018**, *5*, 4896−4902.
(23) Ma, M. L.; Wu, J.; Ning, Y. Q.; Zhou, F.; Yang, M.; Zhang, X.; Zhang, J.; Shang, G. Y. Measurement of gain characteristics of semiconductor lasers by amplified spontaneous emissions from dual facets. *Opt. Express* **2013**, *21*, 10335−10341.
(24) Dudley, J. J.; Crawford, D. L.; Bowers, J. E. Temperature dependence of the properties of DBR mirrors used in surface normaloptoelectronic devices. *IEEE Photonics Technol. Lett.* **1992**, *4*, 311−413.
(25) Young, D. B.; Scott, J. W.; Peters, F. H.; Peters, M. G.; Majewski, M. L.; Thibeault, B. J.; Corzine, S. W.; Coldren, L. A. Enhanced Performance of Offset-Gain High-Barrier Vertical-Cavity Surface-Emitting Lasers. *IEEE J. Quantum Electron.* **1993**, *29*, 2013−2022.
(26) Paul, S.; Roy, J. B.; Basu, P. K. Empirical expressions for the alloy composition and temperature dependence of the band gap and intrinsic carrier density in $Ga_xIn_{1-x}As$. *J. Appl. Phys.* **1991**, *69*, 827−829.

DOI: 10.1021/acsphotonics.9b00406
ACS Photonics 2019, 6, 1990−1995